

Design of transverse electric ring isolators for ultra-low-loss Si_3N_4 waveguides based on the finite element method

Paolo Pintus,^{1,*} Fabrizio Di Pasquale,¹ and John E. Bowers²

¹Scuola Superiore Sant'Anna, 56124, Pisa, Italy

²Department of Electrical and Computer Engineering, University of California, Santa Barbara, California 93106, USA

*Corresponding author: paolo.pintus@sssup.it

Received August 10, 2011; revised October 7, 2011; accepted October 8, 2011;

posted October 19, 2011 (Doc. ID 152540); published November 28, 2011

In this Letter we present the design of a novel (to our best knowledge) integrated TE isolator realized using ultra-low-loss Si_3N_4 waveguides. The device is made of two straight waveguides coupled to an array of ring resonators including a Ce:YIG garnet grown on their internal side. The analysis demonstrates advantages in loss, isolation, and passband width as the number of rings is increased. © 2011 Optical Society of America

OCIS codes: 230.3240, 230.5750, 230.3810.

An optical isolator is one of the most challenging devices to be integrated with high performance [1]. Several solutions have been recently proposed based on nonreciprocal radiation mode conversion [2], nonreciprocal losses [3], interferometric configuration [4], and nonreciprocal phase shift (NRPS) [5]. The more reliable ones are those based on the NRPS [6], where the whole device or a part of it is made of a nonreciprocal material [e.g., magneto-optical (MO) material]. Using this kind of material, photonic crystal isolators [7,8] and ring resonator isolators [6,9] have been recently designed. While the former require high precision and magnetization control over a micrometer scale, the latter are more robust to fabrication errors. Moreover, ring resonators can also be easily thermally tuned to align the isolation bandwidth with the laser wavelength. Recently a TM isolator was realized by bonding a silicon ring resonator with a cerium-substituted yttrium iron garnet (Ce:YIG), obtaining an isolation ratio (IR) of 9 dB [10]. By applying a radial magnetic field to the Ce:YIG, the clockwise (CW) and counterclockwise (CCW) propagation constants are significantly differentiated, allowing for backreflection isolation. One of the main issues of this device is the difficulties in applying a radial magnetic field with a permanent magnet. Further, the smaller the ring, the more difficult is the generation of such a field. Based on recent progress in the realization of low-loss Si_3N_4 waveguides [11], in this Letter we propose and optimize a novel (to our best knowledge) integrated isolator structure for TE modes at 1550 nm. Such waveguides are characterized by ultra low loss (down to 1 dB/m), material stability, and high refractive index regularity. Moreover, the high aspect ratio of these waveguides and their high birefringence increase the polarization maintaining properties reducing the cross-polarization effect, which characterizes high-index-contrast waveguides.

The device we propose is shown in Fig. 1. It is made up of two straight Si_3N_4 waveguides ($n_{\text{Si}_3\text{N}_4} = 1.99$) coupled to an array of ring resonators also made on Si_3N_4 . A Ce:YIG ($n_{\text{Ce:YIG}} = 2.22$, [12]) has been grown on the internal wall of each ring [13]. The whole structure is buried in a silica coating ($n_{\text{SiO}_2} = 1.46$). By applying a vertical magnetostatic field, the resonance wavelength of the rings can be effectively differentiated. When the rings

are on resonance, the light from the input bus [E_1^+ in the upper waveguide in Fig. 1(a)] is coupled to the drop bus [E_1^- in the lower waveguide in Fig. 1(a)]; oppositely, when the light is backreflected from the drop bus, the rings are out of resonance and the input port is isolated.

The mode profile and the resonance wavelength shift have been estimated employing an equivalent straight waveguide with the same ring cross section, as shown in Fig. 1(b). We verified that such approximation provides a small field error (less than 2% on the main component) for a large ring radii ($R \geq 100 \mu\text{m}$). When the external magnetic field is not null, the Ce:YIG relative permittivity tensor is

$$K_{\text{Ce:YIG}} = \begin{pmatrix} n^2 & 0 & 0 \\ 0 & n^2 & 0 \\ 0 & 0 & n^2 \end{pmatrix} + \begin{pmatrix} 0 & 0 & -j\epsilon_{xz} \\ 0 & 0 & 0 \\ j\epsilon_{xz} & 0 & 0 \end{pmatrix}. \quad (1)$$

Considering an external magnetic flux density saturating the Ce:YIG (~ 50 Gauss), the MO effect is described by $\epsilon_{xz} = 7.65 \cdot 10^{-3}$ at $\lambda = 1550$ nm [10,12,14]. To estimate

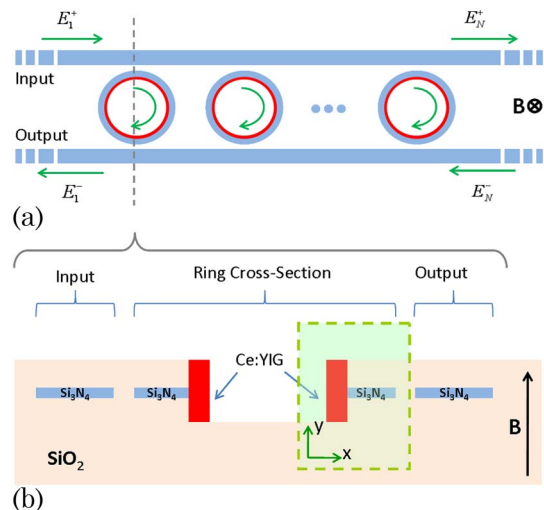


Fig. 1. (Color online) Top view of the (a) isolator and (b) device cross section. The equivalent waveguide cross section has been highlighted.

the difference between the propagation constants in the two directions, we solve the curl-curl equation for the magnetic field \underline{H} using the full vectorial finite element method [14]

$$\nabla \times (K^{-1} \nabla \times \underline{H}) - k_0^2 \underline{H} = 0, \quad (2)$$

where K is the relative permittivity tensor and k_0 is the wavenumber in vacuum. Considering the Cartesian coordinate systems, as shown in Fig. 1(b), the magnetic field is assumed to be of the form

$$\underline{H} = [H_x(x, y)\underline{i}_x + H_y(x, y)\underline{i}_y + jH_z(x, y)\underline{i}_z]e^{j\omega t - j\beta z}. \quad (3)$$

From Eq. (2), we have computed the field H^\pm , the phase constant $\beta^\pm(\lambda)$, and the effective index $n_{\text{eff}}^\pm = \beta^\pm/k_0$ as a function of the wavelength, where the superscript \pm indicates the CW and CCW modes. Note that the different phase velocities in the two directions result into different ring resonance wavelengths. Labeling with λ^+ and λ^- the CW and the CCW resonance wavelengths, the split is $\Delta\lambda = |\lambda^+ - \lambda^-| = \lambda\Delta n_{\text{eff}}/n_g$, where n_g is the average group index with respect to the two directions. To maximize the optical isolation, the minimal ring radius is chosen so that the transmission spectra for the forward and backward resonances are offset by half of the free spectral range $\text{FSR} = \lambda^2/(2\pi R n_g) = 2\Delta\lambda$.

The transfer function of the device is computed using the transfer matrix method [15]. Being κ the ring-waveguide power coupling ratio, we assume a lossless coupler. According to this hypothesis, the field cross coupled and transmission coefficients at the ring-waveguide coupling area are $c = j\sqrt{\kappa}$ and $t = \sqrt{1 - \kappa}$, respectively. Labeling with one the input bus and two the drop bus, the transfer matrices for arbitrary unit cell $M_{\text{UC}i}$ ($i = 1, 2, \dots, N - 1$) and the closing ring M_{CN} are given by

$$M_{\text{UC}i} = \frac{1}{R_{2i}} \begin{pmatrix} (R_{1i}R_{2i} - T_{1i}T_{2i}) \exp(\gamma_{\text{wg}}L) & T_{2i} \exp(\gamma_{\text{wg}}L) \\ -T_{1i} \exp(-\gamma_{\text{wg}}L) & \exp(-\gamma_{\text{wg}}L) \end{pmatrix}, \quad (4a)$$

$$M_{\text{CN}} = \frac{1}{R_{2N}} \begin{pmatrix} (R_{1N}R_{2N} - T_{1N}T_{2N}) & T_{2N} \\ -T_{1N} & 1 \end{pmatrix}, \quad (4b)$$

where R_{1i} , R_{2i} , T_{1i} , and T_{2i} are

$$R_{1i} = \frac{t_{1i} - t_{2i}^*(|t_{1i}|^2 + |c_{1i}|^2) \exp(2\pi R \gamma_{\text{rr}})}{1 - t_{1i}^* t_{2i}^* \exp(2\pi R \gamma_{\text{rr}})}, \quad (5a)$$

$$R_{2i} = \frac{t_{2i} - t_{1i}^*(|t_{2i}|^2 + |c_{2i}|^2) \exp(2\pi R \gamma_{\text{rr}})}{1 - t_{1i}^* t_{2i}^* \exp(2\pi R \gamma_{\text{rr}})}, \quad (5b)$$

$$T_{1i} = -\frac{c_{1i}^* c_{2i} \exp(\pi R \gamma_{\text{rr}})}{1 - t_{1i}^* t_{2i}^* \exp(2\pi R \gamma_{\text{rr}})}, \quad (5c)$$

$$T_{2i} = -\frac{c_{2i}^* c_{1i} \exp(\pi R \gamma_{\text{rr}})}{1 - t_{1i}^* t_{2i}^* \exp(2\pi R \gamma_{\text{rr}})}, \quad (5d)$$

where L is the ring separation, $\gamma_{\text{wg}} = j\beta_{\text{wg}} - \alpha_{\text{wg}}$ is the waveguide propagation constant, β_{wg} and α_{wg} are the waveguide phase and attenuation constants, respectively; similarly, $\gamma_{\text{rr}} = j\beta_{\text{rr}} - \alpha_{\text{rr}}$, β_{rr} , and α_{rr} are the propagation,

phase, and attenuation constants for the ring. In our analysis, we assume that α_{rr} accounts for the bending loss, the scattering loss and the Ce:YIG absorption. The transfer matrix is

$$\begin{pmatrix} E_N^+ \\ E_N^- \end{pmatrix} = M_{\text{CN}} M_{\text{UC}(N-1)} \dots M_{\text{UC}1} \begin{pmatrix} E_1^+ \\ E_1^- \end{pmatrix} \\ = \begin{pmatrix} M_{11} & M_{12} \\ M_{21} & M_{22} \end{pmatrix} \begin{pmatrix} E_1^+ \\ E_1^- \end{pmatrix}. \quad (6)$$

From Eq. (6), the total reflection is

$$R = \left. \frac{E_1^-}{E_1^+} \right|_{E_N^- = 0} = -\frac{M_{21}}{M_{22}}. \quad (7)$$

In order to maximize the resonance wavelength shift $\Delta\lambda$, we consider a 100 nm waveguide thickness and we varied its width and the thickness of the Ce:YIG. Because the refractive index of the Si_3N_4 is smaller than that of the Ce:YIG, the wider the Ce:YIG layer, the more the field is confined in it. When the Ce:YIG is too thick (more than 300 nm), the mode is almost not confined in the Si_3N_4 ring, as can be seen in Fig. 2. Another important issue is the single-mode regime. Let us consider a $100 \text{ nm} \times 2.3 \mu\text{m}$ Si_3N_4 waveguide cross section: the ring is single mode for a Ce:YIG layer thinner than 200 nm, whereas for a wider MO layer, the structure becomes multimodal. In this case, the second-order mode has a maximum closer to the external wall of the ring and it can be coupled easier to the bus with respect to the fundamental mode. To avoid this, we shrink the waveguide down to 900 nm. Figure 3 shows the resonance wavelength split and the field confinement factor in the Ce:YIG by varying the MO-layer thickness. We have identified the optimum configuration considering a $100 \text{ nm} \times 0.9 \mu\text{m}$ Si_3N_4 waveguide cross section and a 300 nm wide Ce:YIG layer. This ensures a wavelength split $\Delta\lambda = 0.307 \text{ nm}$. The minimal radius is $R = 313.9 \mu\text{m}$, with an $\text{FSR} = 0.614 \text{ nm}$.

To compensate for the ring loss, we have fixed the ring-waveguide power coupling coefficient κ , such as $\kappa = [1 - \exp(-2\alpha_{\text{rr}}2\pi R)]/2$, where $[1 - \exp(-2\alpha_{\text{rr}}2\pi R)]$ is the total power cavity loss. In case of low loss, the previous condition can be approximated with $\kappa \sim \alpha_{\text{rr}}2\pi R$, as reported in [14]. Because the optical absorption in the Ce:YIG is less than 4 dB/cm at 1550 nm [16], and the power confinement factor on the MO layer is around 30% (Fig. 3), we considered two possible values for the round trip loss, $\alpha_{\text{rr}} = 1 \text{ dB/cm}$ and $\alpha_{\text{rr}} = 3 \text{ dB/cm}$, which are realistic values for a large ring radius of few hundred micrometers. Assuming $\alpha_{\text{wg}} = 0.1 \text{ dB/cm}$ and $L = \pi R$, the insertion loss (IL), the IR, and the bandwidth at 3 and 10 dB have been computed for different isolator structures with 1, 3, and 10 rings, respectively. The results have been reported in Table 1, while Fig. 4 compares the spectra in cases of 1 ring and 10 rings. It is worth noting that the IL depends more on the coupled power than on α_{rr} . Indeed, the more rings there are, the higher the power coupled between the two buses. Alternately, increasing α_{rr} from 1 dB/cm up to 3 dB/cm, the IL is not significantly affected due to the relatively small ring radius ($\pi R \alpha_{\text{rr}} \approx 0.1 \text{ dB}$, when $\alpha_{\text{rr}} = 1 \text{ dB/cm}$). Besides, as $2\pi R$ is the optical path difference between the rings, the fields interfere constructively at the resonance and the phase response results to be linear.

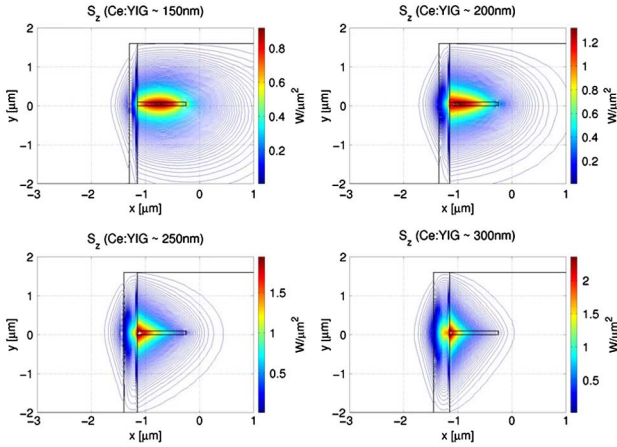


Fig. 2. (Color online) TE Poynting vector for a $100 \text{ nm} \times 0.9 \mu\text{m}$ Si_3N_4 waveguide and four different Ce:YIG layer thicknesses.

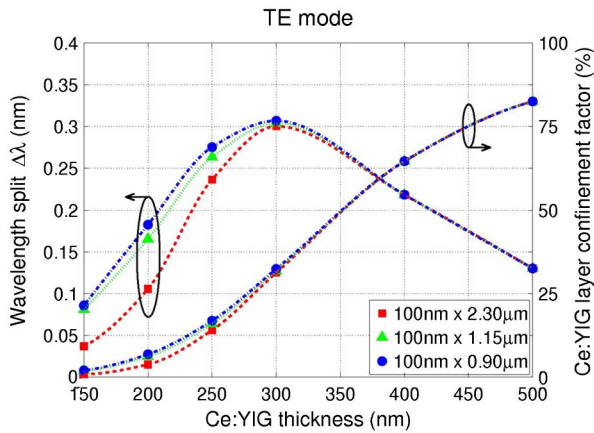


Fig. 3. (Color online) TE wavelength split (left axis) and field confinement factor in the Ce:YIG layer (right axis) with respect to three Si_3N_4 waveguide cross sections and several Ce:YIG layer thickness.

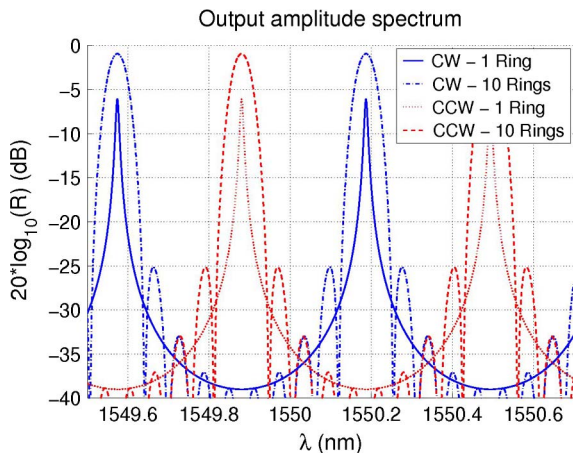


Fig. 4. (Color online) Input-output transfer function R for $\alpha_{\text{tr}} = 1 \text{ dB/cm}$.

As it can be clearly seen from Table 1, increasing the number of rings improves the IR, the isolation bandwidth and decreases the IL. In addition, being the phase response of the device linear in the bandwidth of interest

Table 1. Calculated Device Performance

α_{tr}	Rings	IL	IR	$\text{BW}_{3 \text{ dB}}$	$\text{BW}_{10 \text{ dB}}$
1 dB/cm	1	6.07 dB	32.9 dB	8.5 pm	26.3 pm
	3	2.54 dB	36.4 dB	17.8 pm	53.0 pm
	10	0.90 dB	38.1 dB	50.0 pm	86.3 pm
3 dB/cm	1	6.18 dB	23.5 dB	26.0 pm	79.0 pm
	3	2.60 dB	27.1 dB	54.3 pm	143.0 pm
	10	0.95 dB	28.7 dB	101.0 pm	131.5 pm

($\text{BW}_{3 \text{ dB}}$ and $\text{BW}_{10 \text{ dB}}$), the isolator introduces only a delay without distortion. Note that although a smaller ring radius would reduce the device footprint, too-tiny rings should be avoided in order to limit the bending loss. Moreover, the tolerance fabrication error can be improved using a tapered SCISSOR structure, like in [17].

In conclusion, we have proposed a novel (to our best knowledge) isolator structure and demonstrated advantages in loss, isolation, and passband width. We calculated the high performance of a TE isolator made of ultra-low-loss Si_3N_4 waveguides and Ce:YIG. The device has been optimized considering a ring resonator array, and the most important parameters of the isolator have been computed.

The authors thank Scott Rodgers and Ming-Chun Tien for helpful discussions. This work is supported by the Defense Advanced Research Projects Agency (DARPA) MTO under CIPHER contract no. HR0011-10-1-0079.

References

1. T. R. Zaman, X. Guo, and R. J. Ram, *J. Lightwave Technol.* **26**, 291 (2008).
2. T. Shintaku, *Appl. Phys. Lett.* **73**, 1946 (1998).
3. W. Van Parys, B. Moeyersoon, D. Van Thourhout, R. Baets, M. Vanwolleghem, B. Dagens, J. Decobert, O. Le Gouezigou, D. Make, R. Vanheertum, and L. Lagae, *Appl. Phys. Lett.* **88**, 071115 (2006).
4. T. R. Zaman, X. Guo, and R. J. Ram, *IEEE Photon. Technol. Lett.* **18**, 1359 (2006).
5. J. Fujita, M. Levy, R. M. Osgood, L. Wilkens, and H. Dotsch, *Appl. Phys. Lett.* **76**, 2158 (2000).
6. N. Kono, K. Kakihara, K. Saitoh, and M. Koshiba, *Opt. Express* **15**, 7737 (2007).
7. Z. Wang and S. Fan, *Opt. Lett.* **30**, 1989 (2005).
8. W. Śmigaj, J. Romero-Vivas, B. Gralak, L. Magdenko, B. Dagens, and M. Vanwolleghem, *Opt. Lett.* **35**, 568 (2010).
9. D. Jalas, A. Petrov, M. Krause, J. Hampe, and M. Eich, *Opt. Lett.* **35**, 3438 (2010).
10. M.-C. Tien, T. Mizumoto, P. Pintus, H. Kromer, and J. E. Bowers, *Opt. Express* **19**, 11740 (2011).
11. J. F. Bauters, M. J. R. Heck, D. John, D. Dai, M.-C. Tien, J. S. Barton, A. Leinse, R.-G. Heideman, D. J. Blumenthal, and J. E. Bowers, *Opt. Express* **19**, 3163 (2011).
12. H. Yokoi, *Opt. Mater.* **31**, 189 (2008).
13. T. Uno and S. Noge, *J. Eur. Ceram. Soc.* **21**, 1957 (2001).
14. P. Pintus, M.-C. Tien, and J. Bowers, *Photon. Technol. Lett.* **23**, 1670 (2011).
15. J. Capmany, P. Muñoz, J. D. Domenech, and M. A. Muriel, *Opt. Express* **15**, 10196 (2007).
16. T. Sekijima, H. Itoh, T. Fujii, K. Wakino, and M. Okada, *J. Cryst. Growth* **229**, 409 (2001).
17. P. Bettotti, M. Mancinelli, R. Guider, M. Masi, M. Rao Vanacharla, and L. Pavesi, *Opt. Lett.* **36**, 1473 (2011).